Chapter 10

Defects in Graphene and its Derivatives

Soumyajyoti Haldar and Biplab Sanyal

Additional information is available at the end of the chapter

http://dx.doi.org/10.5772/64297

Abstract

The experimental realization of graphene along with its unique properties in 2004 triggered huge scientific researches in the field of graphene and other two-dimensional (2D) materials. The experimental preparation processes of these materials are prone to defect formation. These defects affect the properties of the pristine system, which can be beneficial or detrimental from the application point of view. In this book chapter, we discuss a few cases of defects in 2D materials such as graphene and its derivatives and their roles in applications.

Keywords: defects in graphene and its derivatives, graphene defects, hybrid materials, gas sensing, *ab initio* theory, magnetism

1. Introduction

The (re)discovery [1, 2] of graphene—a single layer of carbon atoms arranged in a honeycomb lattice—in 2004 by Novoselov et al. has triggered a new aspect of research in two-dimensional (2D) materials [3, 4]. Although the existence of materials with their properties governed by their 2D units was well known for quite some time [5, 6], it is the experimental realization of a single layer graphene has showed that it is possible to exfoliate stable 2D materials from the 3D solids exhibiting various fascinating properties.

A huge number of crystalline solid-state materials having different mechanical, electronic, and transport properties exist from which stable 2D materials can be created due to the presence of weak interaction between the layers [7]. 2D allotropes (e.g., silicene, graphyne, germanene), compounds (e.g., graphane, hexagonal boron nitride, transition metal di-chalcogenides) are the few examples of 2D materials. These 2D materials have the potential for a wide range of applications due to the interesting electronic and structural properties [2, 8–12].

To exploit these various properties, the samples have to be made in a scalable way. Chemical vapor deposition (CVD) has become a very common method for large-scale fabrication. Nonetheless, the CVD samples inevitably contain defects, for example, edges, hetero structures, grain boundaries, vacancies, and interstitial impurities [13–15]. These defects can be seen very easily in transmission electron microscopy (TEM) experiments [16] or scanning tunnelling microscopy (STM) experiments [17]. **Figure 1a**, **b** shows experimental STM and TEM images of an isolated single vacancy in graphene. In the STM image, the single vacancy can be seen as a blob because of increased local density of states. These states appear due to the presence of dangling bonds around the single vacancy.

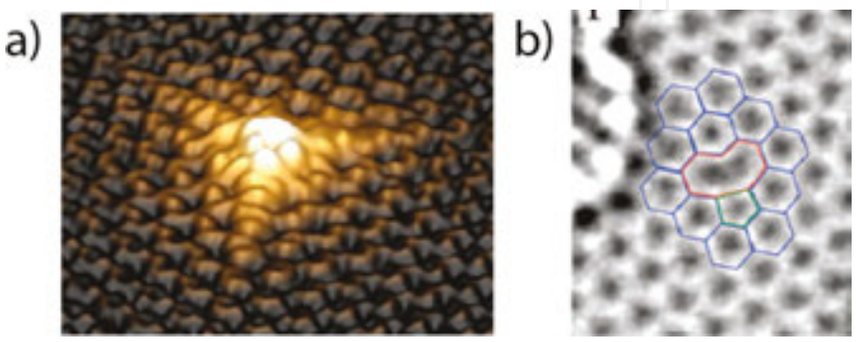

Figure 1. (a) Experimental STM image of single isolated vacancy in graphene. Reprinted with permission from Ugeda et al. [17], copyright (2010) by the American Physical Society. (b) Experimental TEM image of reconstructed single vacancy with atomic configurations. Reprinted (adapted) with permission from Meyer et al. [16], copyright (2008) by the American Chemical Society.

In general, these defects manipulate the properties of the materials and hence their avoidance or deliberate engineering requires a thorough understanding. In one hand, defects can be detrimental to device properties [13], but on the other hand, especially at the nanoscale, defects can bring new functionalities which could be utilized for applications [18, 19].

In this book chapter, we address a few cases of defects in 2D materials such as graphene and its derivatives. We show how one can tune the various properties of the pristine materials with the control insertion of defects in these systems and use them in various applications.

2. Theoretical methods

We have mainly used *ab initio* density functional theory-based methods to calculate various properties of defected 2D materials such as graphene and its derivatives in general. In this section, we will provide a brief introduction to the theoretical methods used.

2.1. Density functional theory

Various different properties of these many-body systems are described by the wave functions associated with it. These wave functions are governed by the time-dependent Schrödinger equation

$$\hat{H}\psi = E\psi \tag{1}$$

where $\hat{H}$ is the Hamiltonian of the many-body systems and represents the energy operator, and E is the total energy of the system. However, one needs various approximations to solve the Schrödinger equation for all kinds of systems.

In density functional theory (DFT), the electron density $n(\vec{r})$ is used to obtain the solution of the Schrödinger equation. The core concept of the DFT is given by two theorems of Hohenberg and Kohn [20], where they showed that the properties of interacting systems can be obtained exactly by the ground state electron density, $n_0(\vec{r})$. Following the two theorems, the total energy of the system can be written as follows:

$$E\left[n\left(\vec{r}\right)\right] = F\left[n\left(\vec{r}\right)\right] + \int V_{ext}\left(\vec{r}\right)n\left(\vec{r}\right)\, d\vec{r} \tag{2}$$

Where functional F represents kinetic energy and all electron-electron interactions. Functional F does not depend on the external potential, and hence, it is same for all the systems. However, Hohenberg-Kohn theorem does not provide any solution toward the exact form of the functional F.

Kohn and Sham [21] gave a way around to obtain the functional F by replacing the interacting many-body system with a non-interacting system consisting of a set of one electron functions (orbitals) while keeping the same ground state. According to the Kohn-Sham formalism, the total energy functional can be written as follows:

$$E\left[n\left(\vec{r}\right)\right] = T_S\left[n\left(\vec{r}\right)\right] + \int V_{ext}\left(\vec{r}\right)n\left(\vec{r}\right)\, d\vec{r} + \frac{1}{2}\iint \frac{n\left(\vec{r_1}\right)n\left(\vec{r_2}\right)}{\left|\vec{r_1} - \vec{r_2}\right|} d\vec{r_1}d\vec{r_2} + E_{XC}\left[n\left(\vec{r}\right)\right] \tag{3}$$

Where T_S is the kinetic energy term of the non-interacting electrons, and V_{ext} is the external potential. The third term in the above equation is the Hartree term representing the classical Coulomb interactions between electrons, and the last term is known as exchange-correlation energy (E_{XC}), which contains all the many-body effects. The formalism of Kohn-Sham is an exact theory. If the form of the E_{XC} is exactly known, then using this formalism, one can calculate the exact ground state of the interacting many-body system.

In reality, the exact form of the exchange-correlation is not trivial, and hence, it is necessary to model the form of the exchange-correlation. Different forms of exchange-correlation can be constructed depending upon various level of approximation, for example, local density approximation (LDA) [20, 22, 23], generalized gradient approximation (GGA) [24–26], hybrid functionals (a mixture of Hartree-Fock and DFT functionals) etc. It is also important to remember that the implementation of single-particle Kohn-Sham equation is not trivial due to the complex behavior of wave functions in different spatial region, for example, in the core

and in the valence region. To describe this complex wave function, a complete basis function is needed which can be of different form, for example, plane waves, localized atomic-like orbitals, Gaussian functions etc.

3. Manipulation of properties of graphene with defects

As mentioned in the introduction, an immense amount of scientific activities is going on in the field of graphene research because of its special properties [27, 28]. However, the lack of band gap limits the usage of graphene in electronic device applications. Therefore, the modification and tuning of graphene properties to open up an energy gap have become a cutting edge research interest among the scientific community. In this section, we show a few examples of manipulating the properties of graphene and hybrid systems with graphene.

3.1. Magnetic impurities in graphene/graphane interface

Graphane—another 2D material—is hydrogenated graphene, where each carbon atom is attached with a hydrogen atom. Unlike graphene, this material is an insulating system with sp^3 hybridization resulting in a large band gap. It is one of the materials, which was first predicted by *ab initio* theory [29] and then latter synthesized in the experiments [30]. Depending upon the concentration of hydrogenation in graphene, semimetal to metal to insulator transition is observed [31]. It has been shown that patterning graphene with partial hydrogenation leads to modification of graphene properties, for example, conducting channels, band gap opening, quantum dots, and magnetically coupled interfaces [31–36]. As a potential material for spintronic applications, graphene/graphane interfaces are of particular interest as these interfaces can mimic the edge properties that can be seen in zigzag or armchair graphene nanoribbons [37–41]. Hence, it will be interesting to study the effect of Fe adatom, as a representative of magnetic impurities, in these hybrid 2D superlattice structures [42].

Figure 2 shows the two different graphene-graphane superlattice structures considered in our calculation. The hydrogen atoms are removed along the diagonal (edge) of the graphane to create armchair (zigzag) graphene-graphane superlattices. We have considered three, five, and seven rows of channel widths for both configurations. In order to find out the stable adsorption site in the graphene channel, we have placed Fe adatom in different places. The analysis of formation energy indicates that the preferred adsorption site for Fe in armchair channel is at the hollow site of graphene channel equidistant from the interface. However, for the zigzag channel, the Fe adatom prefers to bind at a hollow site closer to the interface. Further analysis of energetics as a function of channel width shows that with increasing channel width, the binding energy remains almost constant in the zigzag channel and it decreases in the armchair channel. The calculated value of total magnetic moments for all the systems are ~2.0 $\mu_{B,}$ which is similar to the value of total magnetic moment of Fe adatom substitutionaly placed in graphene [43]. However, the value of onsite local moments is different in both channels and is ~0.5 μ_B higher in the zigzag channel. Our result shows that the binding energy of Fe adatom in the zigzag channels is higher than the binding energy of Fe adatom on pristine graphene

by ~0.2 eV. Hence, we can conclude that the mixed sp^2–sp^3 character of graphene-graphane superlattice helps a strong binding of Fe adatom.

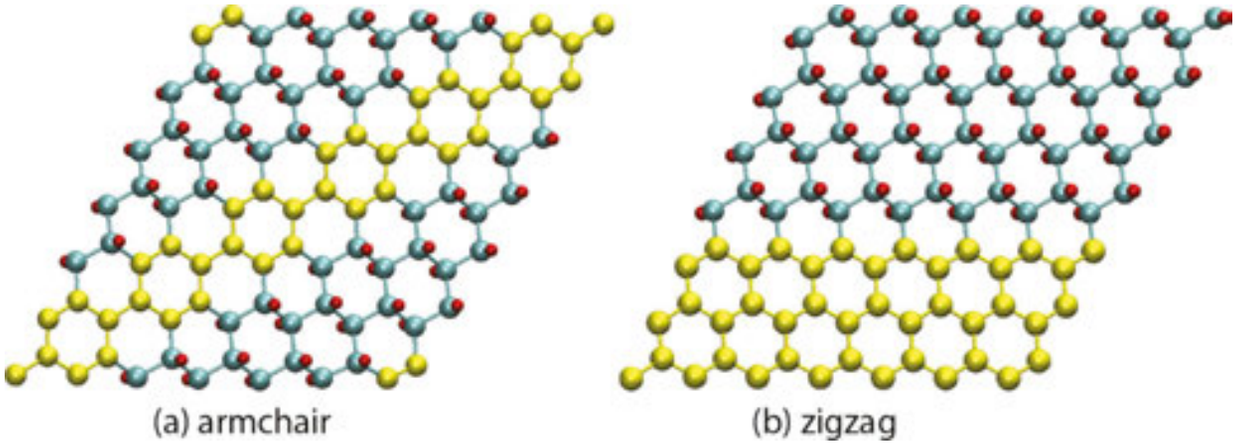

Figure 2. Representative decorations of (a) armchair and (b) zigzag channel in graphane. Reprinted with permission from Haldar et al. [42], copyright (2012) American Physical Society.

Figure 3 shows the total density of states for a single Fe adatom placed on a three-row armchair channel. The analysis of site projected DOS shows that the Fe *d* spin-down electrons induce states below the Fermi energy and reduces the gap quite significantly. Similar features can be observed in the higher row channels although the value of the gap depends on the width.

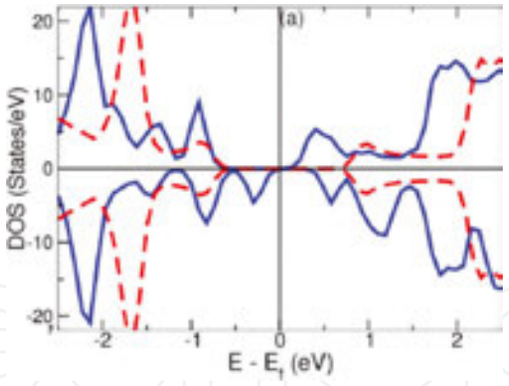

Figure 3. Total DOS of Fe adatom in three-row armchair channel (blue solid line). Total DOS for pristine channel is shown in red dashed line. Reprinted with permission from Haldar et al. [42], copyright (2012) American Physical Society.

The spin density plot of Fe adatom adsorbed in three-row armchair and zigzag channels is shown in **Figure 4**. For armchair channel, it is quite evident from the figure that most of the spin-up density is localized on Fe. The interaction of Fe *d* orbitals with the p_z orbitals of the surrounding C atoms induces polarization in the surrounding C ring, and it induces negative moment on the C atoms. However, in the zigzag channel, the spin density is delocalized and the effect of Fe adatoms can be seen up to fourth nearest neighbor along the interface. The

absorption of Fe adatom in this case reduces the onsite magnetic moments of the edge C atoms. The maximum reduction of this onsite moments can be seen on the nearest site and it can be upto ~15%. In the zigzag channel, the Fe adatom surrounding C atoms ring is not antiferromagnetically ordered and only three C atoms from the same sublattice show significant spin-down densities.

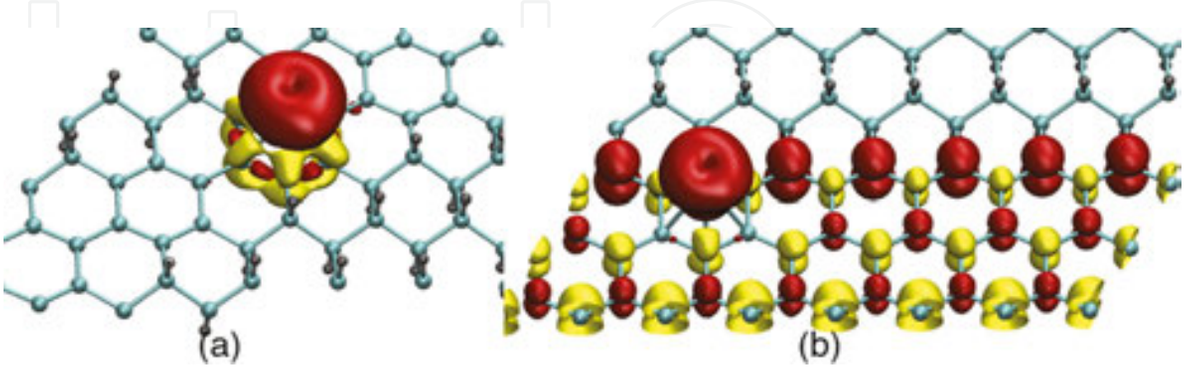

Figure 4. The spin density plot for Fe adatom adsorbed on the three row-armchair and zigzag channel. Reprinted with permission from Haldar et al. [42], copyright (2012) American Physical Society.

We have also calculated the magnetic interactions of two Fe adatoms in these channels. Our result indicates that two Fe adatoms in the armchair channel interact very weakly and hence the exchange energy is also very small favoring an antiferromagnetic interaction. In contrast to the armchair channel, the two Fe adatoms in the zigzag channel interact strongly. A very strong ferromagnetic coupling can be observed in this case between the Fe adatoms, and consequently, they have significantly higher exchange energy compared to the armchair channel.

3.2. Improvement in gas sensing activities

Graphene has also potential application toward the gas sensing properties. This is mainly due to two of the following facts

1. The two-dimensional nature of graphene that consists of only surface and no volume. This feature of graphene enhances the effects of surface dopants.
2. Graphene has a very high conductivity and electrical noise, which enables to detect very small signal changes due to gas molecule absorptions.

Experiments have demonstrated the application of graphene as a solid-state gas sensing device and especially in the detection of single gas molecule, for example, NO_2 [44]. Gaseous molecules act as electron donors or acceptors and modify the carrier density of graphene. Hence, it changes electrical resistance of graphene. Therefore, by measuring the electrical resistance changes, graphene can be used as a gas sensing device [44, 45]. On a pristine graphene lattice, NO_2 molecules are physisorbed. However, chemisorption affects the conduction electron much more than the physisorption. Pristine graphene surface does not have dangling bonds that can chemisorb the gas molecules. However, the presence of defects

can make chemisorption stronger. Hence, in order to increase the gas sensing properties of graphene, one needs to understand the reaction of gas molecules with defected graphene. In this work, we have created defects in graphene using ion beams and studied the gas-sensing properties using current-time measurements, Raman spectroscopy, and gated conductivity characterization [46].

In this study, the graphene flakes were created using the mechanical exfoliation technique on heavily doped Si substrates containing 300 nm SiO_2 top layer. Electron beam lithography was used to fabricate the electrical contacts on device. The defects were created in the pristine graphene by irradiation with 30 keV Ga^+ ions in a vacuum chamber under ~10^{-6} mbar pressure. We have irradiated 20 × 20 μm^2 area and one single irradiation consists of an ion dose of ~10^{12} ions cm^{-2}. We have used a mixture of N_2 and 100-ppm NO_2 gasses as target gas and N_2 gas as a purging gas.

We have used Raman spectroscopy (514 nm wavelength) and atomic force microscopy experiments to determine the thickness of the graphene flakes. From the shape of 2D peak, one can determine the number of layers. **Figure 5** shows the evolution of the Raman spectra with respect to the ion irradiation of graphene. For comparison, the Raman spectrum of the pristine graphene is also shown. Our analysis shows that the graphene flake in this study has a bilayer structure. The D-peak appears at 1352 cm^{-1}, which indicates the formation of defects in graphene. The breathing modes of sp^2 rings cause the appearance of D-peak and only the presence of defects activates it. The intensity of D-peak increases further after the second irradiation and also D′-peak appears at 1626 cm^{-1} which suggest an increase of defects in graphene.

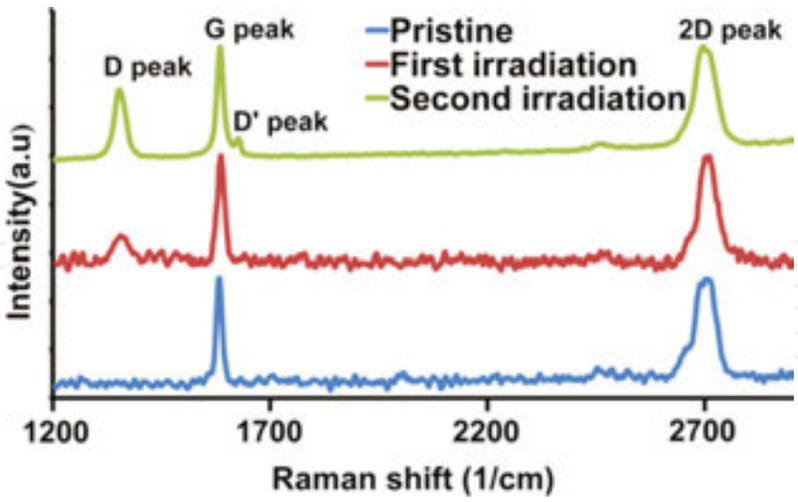

Figure 5. Evolution of Raman spectra with respect to ion irradiation of graphene. Reprinted with permission from Hajati et al. [46], copyright (2012) IOP Publishing.

We have performed gated conductivity experiments to measure the gas sensing properties. **Figure 6** shows the normalized conductance (G/G_0) responses during the exposure of 100 ppm NO_2 in N_2 at room temperature. The conductance of graphene before the exposure is denot-

ed by G_0. The exposure of NO_2 increases the conductance. In pristine graphene, the electrons are transferred from graphene to NO_2 molecules thus increasing the hole density in graphene. A faster response in changing conductance can be observed when the defected graphene (after first irradiation) is exposed to NO_2 gas. These show higher sensitivity to NO_2 gas when compared to the pristine graphene. However, the gas sensing properties decrease after the second irradiation due to the increase of defects, which increases the number of scattering states. Hence, it reduces the conductance.

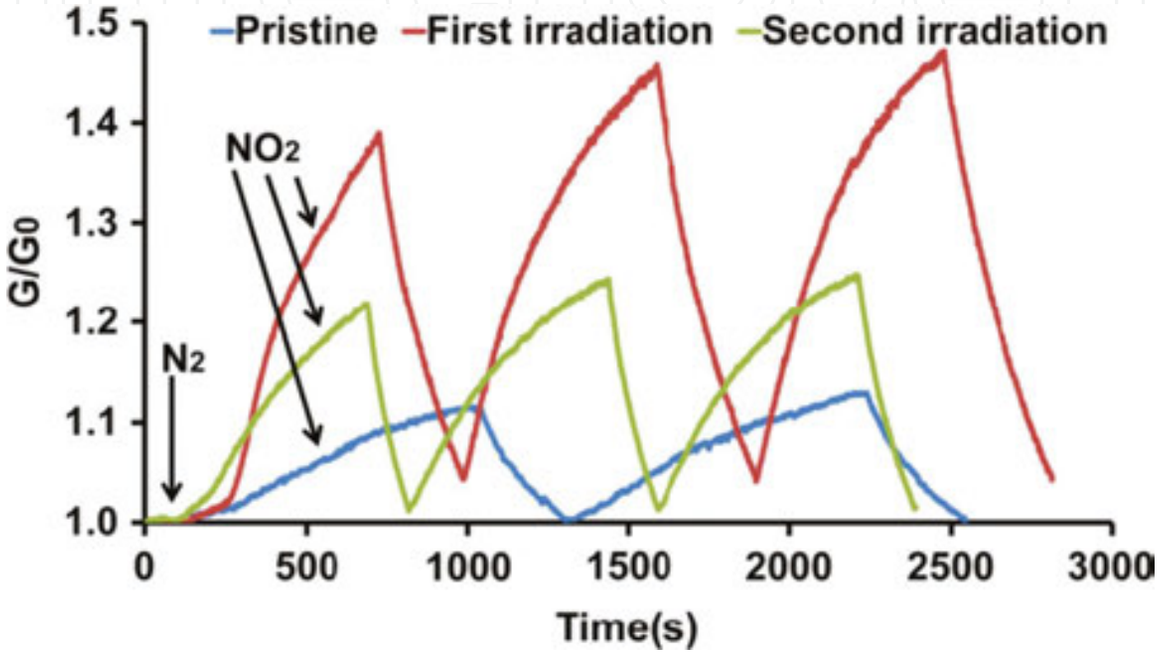

Figure 6. Normalized conductance (G/G_0) response of the graphene gas sensor. The exposure of the NO_2 gas started after 110 s in all three cases. The average rise times for pristine, first, and second defected graphene (during NO_2 exposure) are 500, 328, and 420 s respectively. Reprinted with permission from Hajati et al. [46], copyright (2012) IOP Publishing.

We have also performed *ab initio* density functional calculations in order to understand the interactions between NO_2 and defected graphene. We have used a monolayer graphene for our calculation as most of the defects are same in both monolayer and bilayer graphene. We have studied the binding of NO_2 gas with graphene with different defects, for example, monovacancy, divacancy (585 defect), 686 structure [47], and Stone-Wales (SW) defect. Our analysis shows that the SW vacancy has the highest binding energy with NO_2 molecule (0.72 eV) when compared to the other defects where binding energies are ~0.3 eV.

In **Figure 7**, we have shown the total and molecular NO_2 spin polarized DOS, inverse participation ratio (IPR) [48] for the electronic states of SW + NO_2. The calculated DOS shows that the spin-polarized molecular levels of NO_2 molecules appear near the Fermi energy. These cause 1 μ_B/unit cell magnetic moments. We have also calculated the IPR, which is inversely proportional to the number of atoms contributing to a particular molecular orbital, and hence, IPR gives a quantitative characterization of localization of molecular orbitals. In **Figure 7**, the

http://dx.doi.org/10.5772/64297

calculated IPR has very small values near the Fermi energy, which shows conducting character of the states.

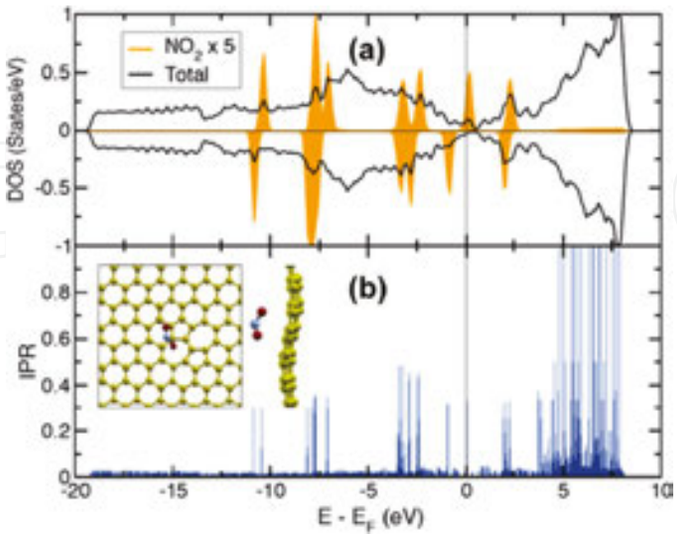

Figure 7. (a) Total and molecular NO_2 spin polarized DOS. (b) Inverse participation ratio (IPR) for the electronic states of SW + NO_2. (b) Optimized geometry of NO_2 at SW-defect site in the graphene lattice is shown as top and side views. Reprinted with permission from Hajati et al. [46]. Copyright (2012) IOP Publishing.

3.3. Fluorination of graphene using defect insertion

Functionalization of graphene has attracted significant attention as it has the potential to make graphene useful for applications. Functionalization of graphene by fluorination is one of the

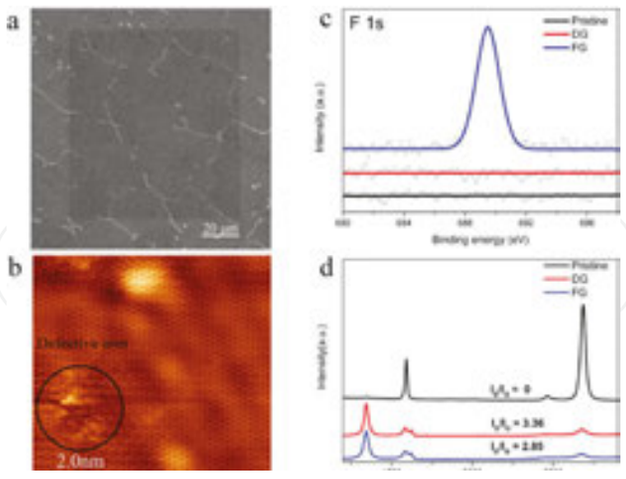

Figure 8. Characterization of pristine graphene, defected graphene (DG) and fluorinated graphene (FG). (a) Scanning electron microscope (SEM) image of local functionalization of graphene (100 μm × 100 μm) with ion doses of 10^{13} ions/cm^2 and simultaneous 167 s gas exposure. (b) Scanning tunneling microscopy image of DG under the same ion dosage. (c) X-ray photoelectron spectroscopy spectra of F 1 s peak of pristine graphene, DG and FG. FG reveals a distinguished F 1 s peak, and the F 1 s spectrum of pristine graphene as well as DG is given as a reference. (d) Raman comparison of pristine graphene, DG and FG. Lower ID/IG in FG in contrast to DG indicates lower degree of defects density and larger crystalline size. Reprinted with permission from Li et al. [49].

ways. In general, the functionalization of graphene is a challenging process. Local functionalization is a promising tool to keep the desired properties of graphene intact after the modification. In this section, we discuss an interesting technique, which allows precise site-selective fluorination [49].

We have used a focused ion beam irradiation under XeF_2 environment in high vacuum to design the site-selective fluorination. In this method, the graphene surface is locally radicalized using high-energy ion irradiation under fluorine contained precursor molecule environment. We have used X-ray photoelectron spectroscopy (XPS), Raman spectroscopy, scanning tunnelling microscopy (STM), and density functional theory (DFT) calculations to verify the fluorination process and explain the mechanism.

The defected structures shown in **Figure 8a**, **b** are obtained by irradiating graphene locally with high-energy (30 kV) Ga^+ ions with an irradiation dose of 10^{13} ions cm^{-2}. Under this amount of irradiation dose, graphene retains most of its lattice structure. However, the damaged part shows significant defect formations, which are mainly vacancies. The formation of fluorinated graphene can be seen from **Figure 8c**, where XPS shows a clear signal of F 1 s peak. We have also used Raman spectroscopy to find out the structural information. From the Raman spectroscopy figure (**Figure 8d**), we can see that the intensity of the D-peak (at 1350 cm^{-1}) increases after irradiation and the intensity of the 2D-peak decreases sharply. It means that the translational symmetry of sp^2 bond is broken. Compared to the defected graphene, in fluorinated graphene, the ratio of D and G peak (I_D/I_G) is lower. This implies that fluorinated graphene contains less structural disorder.

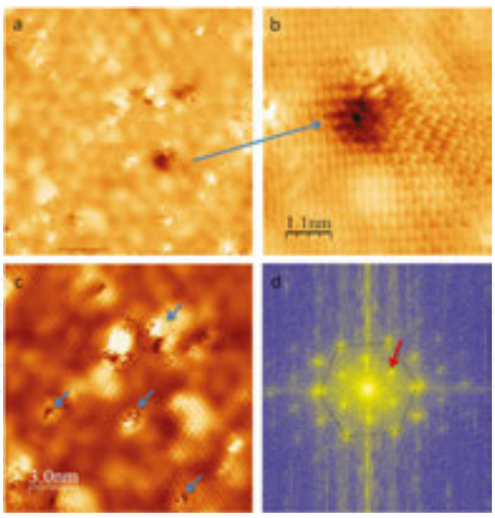

Figure 9. STM images of fluorinated graphene. (a) 20 × 20 nm^2 area. (b) Zoom in image of a hole defect showing standing waves pattern. (c) Other area 15 × 15 nm^2 showing bright feature decorating holes (blue arrows) attributed to fluorine atoms. (d) FFT of (a). It reveals the first Brillouin zone with hexagonal lattice and K points (red arrows) associated to the standing waves pattern due to intervalley scattering. Reprinted with permission from Li et al. [49].

STM experiments were carried out on the fluorinated graphene for a better understanding of structures. **Figure 9** shows these images, which are taken at low bias voltage of −75 mV at Fermi

level. In **Figure 9a**, a 20 × 20 nm^2 area of fluorinated graphene is shown. The surface is covered by various defects, corrugations, etc. Standing waves with different structures near the defect area form these corrugations. The Fast Fourier transformation of **Figure 9a** is shown in **Figure 9d**, which clearly shows the first Brillouin zone of the hexagonal lattice and the K points. These K points are related to the standing waves pattern from the intervalley scattering [50]. All the defects in the surface are connected with the standing waves. Larger defects (zoomed in **Figure 9b**) show standing waves as straight lines similar to as observed in step edges. Thus, it can be concluded that the fluorinated graphene remains metallic [51]. In **Figure 9c**, the bright features are associated with the fluorine atoms. Combining the observation of standing waves related to delocalized electron at the conjugated sp^2 bonds from **Figure 9b**, it could be concluded that the fluorination happens near the defect sites created by the ion irradiation.

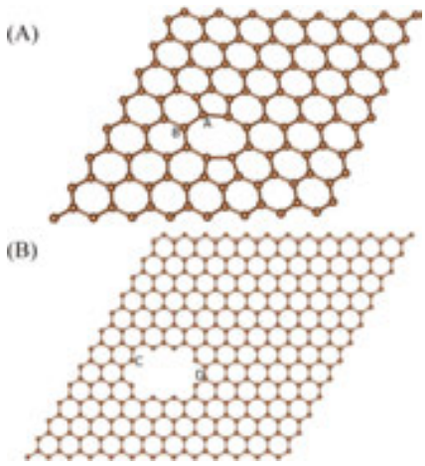

Figure 10. *Ab initio* density functional theory (DFT) calculation models of fluorinated graphene. Di-vacancy model (a) and hole-defect model (b), 0.95 nm in length, are based on the STM observation. Binding energies are shown in **Table 1**.

Structure	E_{abs} (eV)	Hybridization
Pristine	−1.91	sp^3
Di-vacancy at site A	−2.86	sp^3
Di-vacancy at site B	−2.25	sp^3
Hole-defect site C	−5.64	sp^2
Hole-defect site D	−2.18	sp^3

Reprinted with permission from Li et al. [49].

Table 1. Adsorption energies of fluorine adatom on pristine graphene as well as the edge carbon atoms surrounding the two defects.

We have also performed *ab initio* density functional-based calculations to find out fluorine adsorption characteristics on defected graphene. We have used two models of defected

graphene for our calculations as shown in **Figure 10**. These models are: (i) divacancy model and (ii) hole-defect model. These are the two types of models that can be seen in the STM images. In these two types of defects, there are only four possible places for single fluorine adatoms to be adsorbed. These four places are marked as site A–D. In **Table 1**, we have tabulated the energetics. Our calculations show that the adsorption energy of the fluorine adatom on pristine graphene is very high compared to the di-vacancy and the hole defects. It implies that the fluorine atoms are prone to react with the carbon atom surrounding the defect sites. At site C, the carbon atom is radicalized due to the presence of dangling bonds and hence has very low adsorption energy for fluorine adsorption. In this case, the C–F bond is planar with a bond length of 0.136 nm, typical for sp^2 hybridization. The C–F bonds in other sites are all out of plane (perpendicular to the graphene lattice) and have sp^3 hybridization. This strong bond between dangling bond and fluorine atoms implies that different gases could be utilized to functionalize graphene.

In conclusion, we have showed an experimental technique to design site-selective local fluorination using high kinetic energy ion irradiation and simultaneous XeF_2 gas injection. Our method opens up a possibility of functionalize graphene locally with a wide range of other functional materials.

4. Conclusion

From the discussions of Fe adatom adsorption at the partially hydrogenated channels, we conclude that the magnetic adatoms in the zigzag channel interact quite substantially as compared to the armchair channel. The response of the two channels in the presence of magnetic impurities is quite different, viz., localized (delocalized) in the armchair (zigzag) channel. In the semiconducting armchair channel, the magnetic coupling is weakly antiferromagnetic. However, in the delocalized zigzag channel, a relatively stronger ferromagnetic coupling can be observed. Hence, it may be possible to design magnetic graphene lattice by depositing suitable magnetic impurities by means of scanning tunneling microscopy tips, which can lead to the possibility of designing ultrathin magnetic devices.

We have also studied how defects in graphene affect the gas sensing properties. The defects are created using the Ga^+ ion irradiation. The defected graphene shows higher conductivity changes in the presence of NO_2 gas when compared to the pristine graphene. Hence, one can conclude that the defected graphene has higher sensitivity in gas detection. The NO_2 gas molecules bind strongly with SW defects in graphene, which changes the local electronic structure and enhance the transport properties.

We have also demonstrated how defects in graphene can be used for various important applications, for example, spintronics and gas sensing. The presence of defects modifies the structural and electronic properties of the 2D material as well as the binding entities. The understanding of these phenomena can be achieved by materials specific theoretical methods. From the experimental side, the controlled nanoengineering of defects may lead to novel applications and should be pursued seriously in near future.

Author details

Soumyajyoti Haldar and Biplab Sanyal*

*Address all correspondence to: Biplab.Sanyal@physics.uu.se

Department of Physics and Astronomy, Uppsala University, Uppsala, Sweden

References

[1] May JW: Platinum surface LEED rings. Surf Sci. 1969;17:267–270.

[2] Novoselov KS, Geim AK, Morozov SV, Jiang D, Zhang Y, Dubonos SV, et al.: Electric field effect in atomically thin carbon films. Science. 2004;306:666–669. doi:10.1126/science.1102896

[3] Novoselov KS, Jiang D, Schedin F, Booth TJ, Khotkevich VV, Morozov SV, et al.: Two-dimensional atomic crystals. Proc Natl Acad Sci USA. 2005;102:10451–10453. doi:10.1073/pnas.0502848102

[4] Butler SZ, Hollen SM, Cao L, Cui Y, Gupta JA, Gutiérrez HR, et al.: Progress, challenges, and opportunities in two-dimensional materials beyond graphene. ACS Nano. 2013;7:2898–2926. doi:10.1021/nn400280c

[5] Wilson JA, Yoffe AD: The transition metal dichalcogenides discussion and interpretation of the observed optical, electrical and structural properties. Adv Phys. 1969;18:193–335. doi:10.1080/00018736900101307

[6] Bednorz JG, Müller KA: Possible high Tc superconductivity in the Ba–La–Cu–O system. Zeitschrift für Physik B Condensed Matter. 1986;64:189–193. doi:10.1007/BF01303701

[7] Gibney E: 2D or not 2D. Nature. 2015;522:274–276. doi:10.1038/522274a

[8] Watanabe K, Taniguchi T, Kanda H: Direct-bandgap properties and evidence for ultraviolet lasing of hexagonal boron nitride single crystal. Nat Mater. 2004;3:404–409. doi:10.1038/nmat1134

[9] Georgiou T, Jalil R, Belle BD, Britnell L, Gorbachev RV, Morozov SV, et al.: Vertical field-effect transistor based on graphene-WS 2 heterostructures for flexible and transparent electronics. Nat Nanotechnol. 2013;8:100–103. doi:10.1038/nnano.2012.224

[10] Feliciano GT, Sanz-Navarro C, Coutinho-Neto MD, Ordejon P, Scheicher RH, Rocha AR: Capacitive DNA detection driven by electronic charge fluctuations in a graphene nanopore. Phys Rev Appl. 2015;3:034003–034007. doi:10.1103/PhysRevApplied.3.034003

[11] Le Lay G: 2D materials: silicene transistors. Nat Nanotechnol. 2015;10:202–203. doi: 10.1038/nnano.2015.10

[12] Prasongkit J, Amorim RG, Chakraborty S, Ahuja R, Scheicher RH, Amornkitbamrung V: Highly sensitive and selective gas detection based on silicene. J Phys Chem C. 2015;119:16934–16940. doi:10.1021/acs.jpcc.5b03635

[13] Song HS, Li SL, Miyazaki H, Sato S, Hayashi K, Yamada A, et al.: Origin of the relatively low transport mobility of graphene grown through chemical vapor deposition. Sci Rep. 2012;2:337. doi:10.1038/srep00337

[14] Niu T, Zhou M, Zhang J, Feng Y, Chen W: Growth intermediates for CVD graphene on Cu(111): carbon clusters and defective graphene. J Am Chem Soc. 2013;135:8409–8414. doi:10.1021/ja403583s

[15] Banhart F, Kotakoski J, Krasheninnikov AV: Structural defects in graphene. ACS Nano. 2011;5:26–41. doi:10.1021/nn102598m

[16] Meyer JC, Kisielowski C, Erni R, Rossell MD, Crommie MF, Zettl A: Direct imaging of lattice atoms and topological defects in graphene membranes. Nano Lett. 2008;8:3582–3586. doi:10.1021/nl801386m

[17] Ugeda MM, Brihuega I, Guinea F, Gómez-Rodríguez JM: Missing atom as a source of carbon magnetism. Phys Rev Lett. 2010;104:096804. doi:10.1103/PhysRevLett. 104.096804

[18] Rocha AR, Martins TB, Fazzio A, Da Silva AJR: Disorder-based graphene spintronics. Nanotechnology. 2010;21:345202. doi:10.1088/0957-4484/21/34/345202

[19] Xu C, Luo G, Liu Q, Zheng J, Zhang Z, Nagase S, et al.: Giant magnetoresistance in silicene nanoribbons. Nanoscale. 2012;4:3111–3117. doi:10.1039/c2nr00037g

[20] Hohenberg P, Kohn W: Inhomogeneous electron gas. Phys Rev. 1964;136:B864–B871. doi:10.1103/PhysRev.136.B864

[21] Kohn W, Sham LJ: Self-consistent equations including exchange and correlation effects. Phys Rev. 1965;140:A1133–A1138. doi:10.1103/physrev.140.a1133

[22] Perdew JP, Zunger A: Self-interaction correction to density-functional approximations for many-electron systems. Phys Rev B. 1981;23:5048–5079. doi:10.1103/ PhysRevB.23.5048

[23] Ceperley DM, Alder BJ: Ground state of the electron gas by a stochastic method. Phys Rev Lett. 1980;45:566–569. doi:10.1103/PhysRevLett.45.566

[24] Perdew JP, Chevary JA, Vosko SH, Jackson KA, Pederson MR, Singh DJ, et al.: Atoms, molecules, solids, and surfaces: applications of the generalized gradient approximation for exchange and correlation. Phys Rev B. 1992;46:6671–6687. doi:10.1103/ PhysRevB.46.6671

[25] Perdew JP, Burke K, Ernzerhof M: Generalized gradient approximation made simple. Phys Rev Lett. 1996;77:3865–3868. doi:10.1103/PhysRevLett.77.3865

[26] Perdew JP, Burke K, Ernzerhof M: Generalized gradient approximation made simple [Phys. Rev. Lett. 77, 3865 (1996)]. Phys Rev Lett. 1997;78:1396–1396. doi:10.1103/PhysRevLett.78.1396

[27] Geim AK, Novoselov KS: The rise of graphene. Nat Mater. 2007;6:183–191. doi:10.1038/nmat1849

[28] Castro Neto AH, Guinea F, Peres NMR, Novoselov KS, Geim AK: The electronic properties of graphene. Rev Mod Phys. 2009;81:109–162. doi:10.1103/RevModPhys.81.109

[29] Sofo JO, Chaudhari AS, Barber GD: Graphane: a two-dimensional hydrocarbon. Phys Rev B. 2007;75:153401-153404. doi:10.1103/PhysRevB.75.153401

[30] Elias DC, Nair RR, Mohiuddin TMG, Morozov SV, Blake P, Halsall MP, et al.: Control of graphene's properties by reversible hydrogenation: evidence for graphane. Science. 2009;323:610–613. doi:10.1126/science.1167130

[31] Chandrachud P, Pujari BS, Haldar S, Sanyal B, Sanyal B, Kanhere DG: A systematic study of electronic structure from graphene to graphane. J Phys: Condens Matter. 2010;22:465502. doi:10.1088/0953-8984/22/46/465502

[32] Singh AK, Yakobson BI: Electronics and magnetism of patterned graphene nanoroads. Nano Lett. 2009;9:1540–1543. doi:10.1021/nl803622c

[33] Sessi P, Guest JR, Bode M, Guisinger NP: Patterning graphene at the nanometer scale via hydrogen desorption. Nano Lett. 2009;9:4343–4347. doi:10.1021/nl902605t

[34] Lu YH, Feng YP: Band-gap engineering with hybrid graphane–graphene nanoribbons. J Phys Chem C. 2009;113:20841–20844. doi:10.1021/jp9067284

[35] Balog R, Jørgensen B, Nilsson L, Andersen M, Rienks E, Bianchi M, et al.: Bandgap opening in graphene induced by patterned hydrogen adsorption. Nat Mater. 2010;9:315–319. doi:10.1038/nmat2710

[36] Ao ZM, Hernández-Nieves AD, Peeters FM, Li S: Enhanced stability of hydrogen atoms at the graphene/graphane interface of nanoribbons. Appl Phys Lett. 2010;97:233109. doi:10.1063/1.3525377

[37] Nakada K, Fujita M, Dresselhaus G, Dresselhaus MS: Edge state in graphene ribbons: nanometer size effect and edge shape dependence. Phys Rev B. 1996;54:17954–17961. doi:10.1103/PhysRevB.54.17954

[38] Koskinen P, Malola S, Häkkinen H: Evidence for graphene edges beyond zigzag and armchair. Phys Rev B. 2009;80:073401. doi:10.1103/PhysRevB.80.073401

[39] Jia X, Hofmann M, Meunier V, Sumpter BG, Campos-Delgado J, Romo-Herrera JM, et al.: Controlled formation of sharp zigzag and armchair edges in graphitic nanoribbons. Science. 2009;323:1701–1705. doi:10.1126/science.1166862

[40] Girit ÇÖ, Meyer JC, Erni R, Rossell MD, Kisielowski C, Yang L, et al.: Graphene at the edge: stability and dynamics. Science. 2009;323:1705–1708. doi:10.1126/science.1166999

[41] Koskinen P, Malola S, Häkkinen H: Self-passivating edge reconstructions of graphene. Phys Rev Lett. 2008;101:115502. doi:10.1103/PhysRevLett.101.115502

[42] Haldar S, Kanhere DG, Sanyal B: Magnetic impurities in graphane with dehydrogenated channels. Phys Rev B: Condensed Matter and Mater Phys. 2012;85:155426. doi: 10.1103/PhysRevB.85.155426

[43] Valencia H, Gil A, Frapper G: Trends in the adsorption of 3d transition metal atoms onto graphene and nanotube surfaces: a DFT study and molecular orbital analysis. J Phys Chem C. 2010;114:14141–14153. doi:10.1021/jp103445v

[44] Schedin F, Geim AK, Morozov SV, Hill EW, Blake P, Katsnelson MI, et al.: Detection of individual gas molecules adsorbed on graphene. Nat Mater. 2007;6:652–655. doi: 10.1038/nmat1967

[45] Zhu Y, Murali S, Cai W, Li X, Suk JW, Potts JR, et al.: Graphene and graphene oxide: synthesis, properties, and applications. Adv Mater. 2010;22:3906–3924. doi:10.1002/adma.201001068

[46] Hajati Y, Blom T, Jafri SHM, Haldar S, Bhandary S, Shoushtari MZ, et al.: Improved gas sensing activity in structurally defected bilayer graphene. Nanotechnology. 2012;23:505501. doi:10.1088/0957-4484/23/50/505501

[47] Appelhans DJ, Carr LD, Lusk MT: Embedded ribbons of graphene allotropes: an extended defect perspective. New J Phys. 2010;12. doi:10.1088/1367-2630/12/12/125006

[48] Atta-Fynn R, Biswas P, Ordejon P, Drabold D: Systematic study of electron localization in an amorphous semiconductor. Phys Rev B. 2004;69:085207–085210. doi:10.1103/PhysRevB.69.085207

[49] Li H, Daukiya L, Haldar S, Lindblad A, Sanyal B, Eriksson O, et al.: Site-selective local fluorination of graphene induced by focused ion beam irradiation. Sci Rep. 2016;6:19719. doi:10.1038/srep19719

[50] Simon L, Bena C, Vonau F, Cranney M, Aubel D: Fourier-transform scanning tunnelling spectroscopy: the possibility to obtain constant-energy maps and band dispersion using a local measurement. J Phys D: Appl Phys. 2011;44:464010. doi: 10.1088/0022-3727/44/46/464010

[51] Yang H, Mayne AJ, Boucherit M, Comtet G, Dujardin G, Kuk Y: Quantum interference channeling at graphene edges. Nano Lett. 2010;10:943–947. doi:10.1021/nl9038778